

Probing Electronic Motion and Core Potential by Coulomb-reshaped Terahertz Radiation

Ziyang Gan,[†] Kaixuan Zhang,[§] Yuan Gao,[†] Ahai Chen,[‡] Yizhu Zhang,^{*,||} Tian-Min
Yan,^{*,†} Thomas Pfeifer,[⊥] and Yuhai Jiang^{*,‡}

[†]*Shanghai Advanced Research Institute, Chinese Academy of Sciences, Shanghai 201210,
China*

[‡]*Center for Transformative Science, School of Physical Science and Technology,
ShanghaiTech University, Shanghai 201210, China*

[¶]*University of Chinese Academy of Sciences, Beijing 100049, China*

[§]*Zhejiang Provincial Key Laboratory of Ultra-Weak Magnetic-Field Space and Applied
Technology, Hangzhou Innovation Institute, Beihang University, Hangzhou 310051, China*

^{||}*Center for Terahertz Waves and College of Precision Instrument and Optoelectronics
Engineering, Key Laboratory of Opto-electronics Information and Technical Science,
Ministry of Education, Tianjin University, Tianjin 300350, China*

[⊥]*Max-Planck Institute for Nuclear Physics, Heidelberg 69117, Germany*

E-mail: zhangyizhu@tju.edu.cn; yantm@sari.ac.cn; jiangyh3@shanghaitech.edu.cn

Abstract

The nature of electronic motion and structural information of atoms and molecules is encoded into strong-field induced radiations ranging from terahertz (THz) to extreme ultraviolet wavelength. The dependence of THz yields in bi-chromatic laser fields on ellipticity and interpulse phase delay were experimentally measured, and the trajectory calculations establish the link between the THz emission and the motion of the

photoelectron wave packet. The interaction between the photoelectron and parent core transforms from soft collision to recollision as the laser field tuned from elliptical to linear polarization, which can be reflected in THz emission. The soft collision is found to be more effective in reconstructing electron dynamics through THz polarization, which enables to construct the effective core potential of the generating medium with the Coulomb-reshaped THz radiation in an elliptically polarized laser field. Our work allows designing innovative all-optical THz measurements of electronic and structural dynamics.

Introduction

Strong-field induced radiation ranging from terahertz (THz) to extreme ultraviolet wavelength contain a wealth of structural and dynamical information of the generating medium. The high-harmonic generation (HHG) of extreme ultraviolet photons has been widely used for molecular orbital tomography^{1,2}, and the probing of electron wave packet^{3,4}, nuclear dynamics and structural rearrangement on a subfemtosecond time scale⁵⁻⁷. Analogous to HHG, the THz wave generation (TWG)⁸, so-called zeroth-order Brunel harmonics⁹, has been also considered as an all-optical approach for probing molecular structures¹⁰, and recently an innovative optical attoclock¹¹ where the THz polarization direction acts as a "clock hand" for mapping the tunneling delay, laterally complementing to currently used attoclock implemented by photoelectron momentum spectroscopy¹²⁻¹⁵.

The strong-field induced TWG physically originates from the acceleration of tunneling photoelectron wave packet in oscillating electric field, described macroscopically by the photo-current (PC) model¹⁶, or microscopically by continuum-continuum transition in strong field approximation^{17,18}. In typical scenarios, when fitting the macroscopic THz yield, the aforementioned models neglecting the Coulomb interaction between the free electron and the parent core suffices. Nevertheless, when employing all-optical THz probing to investigate microscopic structures and electron dynamics, the Coulomb effects becomes highly

sensitive and thus necessitates careful consideration.

The Coulomb influence on photoelectron momentum spectra and HHGs, when retrieving the photoelectron dynamics, has been fully noticeable. When measuring the electron tunneling delay implemented by attoclock¹³⁻¹⁵, all the works emphasized that, the Coulomb interaction must be taken into account, and the tunneling delay has to be correctly disentangled from the final photoelectron momentum spectra to achieve a meaningful quantitative interpretation. The Coulomb-reshaped electronic wave packet has been encoded in the phase of HHGs¹⁹, which affects the accuracy of structural tomography^{2,20,21}. For TWGs, the involvement of Coulomb potential in microscopic information extraction, as well as the speculation on photoelectron motion and structural information, has been rarely investigated.

Although the TWG has been well described by the PC model^{16,22}, where the net residual photocurrent density plays the core role, the photocurrent lacks more fine-grained microscopic information of photoelectron dynamics. As the photocurrent is essentially a macroscopic correspondence of asymmetric photoelectron wave packet conceptually described by an ensemble of propagating photoelectron trajectories^{23,24}, the TWG can be evaluated from microscopic trajectories to account for the influence from both the external field $\mathbf{E}(t)$ and the potential of the parent ion $V(\mathbf{r})$ ²⁵. This influence is experimentally substantiated by measuring the optimal THz yields as a function of two-color phase delay²⁵, as well as by examining the THz polarization under specific polarization combinations of two-color fields²⁶.

In this work, according to the classical trajectory Monte-Carlo (CTMC) method, we elucidate how various types of electron-core interactions, including soft collisions and recollisions, are imprinted in the TWG polarization. Meanwhile, it reveals the equivalence between the THz polarization and asymmetry pointer of photoelectron momentum distributions (PMDs), which can be substantially employed for the reconstruction of atomic core potentials.

Strong-field induced radiation ranging from terahertz (THz) to extreme ultraviolet wavelength contain a wealth of structural and dynamical information of the generating medium.

The high-harmonic generation (HHG) of extreme ultraviolet photons has been widely used for molecular orbital tomography^{1,2}, and the probing of electron wave packet^{3,4}, nuclear dynamics and structural rearrangement on a subfemtosecond time scale⁵⁻⁷. Analogous to HHG, the THz wave generation (TWG)⁸, so-called zeroth-order Brunel harmonics⁹, has been also considered as an all-optical approach for probing molecular structures¹⁰, and recently an innovative optical attoclock¹¹ where the THz polarization direction acts as a "clock hand" for mapping the tunneling delay, laterally complementing to currently used attoclock implemented by photoelectron momentum spectroscopy¹²⁻¹⁵.

The strong-field induced TWG physically originates from the acceleration of tunneling photoelectron wave packet in oscillating electric field, described macroscopically by the photo-current (PC) model¹⁶, or microscopically by continuum-continuum transition in strong field approximation^{17,18}. In typical scenarios, when fitting the macroscopic THz yield, the aforementioned models neglecting the Coulomb interaction between the free electron and the parent core suffices. Nevertheless, when employing all-optical THz probing to investigate microscopic structures and electron dynamics, the Coulomb effects becomes highly sensitive and thus necessitates careful consideration.

The Coulomb influence on photoelectron momentum spectra and HHGs, when retrieving the photoelectron dynamics, has been fully noticeable. When measuring the electron tunneling delay implemented by attoclock¹³⁻¹⁵, all the works emphasized that, the Coulomb interaction must be taken into account, and the tunneling delay has to be correctly disentangled from the final photoelectron momentum spectra to achieve a meaningful quantitative interpretation. The Coulomb-reshaped electronic wave packet has been encoded in the phase of HHGs¹⁹, which affects the accuracy of structural tomography^{2,20,21}. For TWGs, the involvement of Coulomb potential in microscopic information extraction, as well as the speculation on photoelectron motion and structural information, has been rarely investigated.

Although the TWG has been well described by the PC model^{16,22}, where the net residual photocurrent density plays the core role, the photocurrent lacks more fine-grained micro-

scopic information of photoelectron dynamics. As the photocurrent is essentially a macroscopic correspondence of asymmetric photoelectron wave packet conceptually described by an ensemble of propagating photoelectron trajectories^{23,24}, the TWG can be evaluated from microscopic trajectories to account for the influence from both the external field $\mathbf{E}(t)$ and the potential of the parent ion $V(\mathbf{r})$ ²⁵. This influence is experimentally substantiated by measuring the optimal THz yields as a function of two-color phase delay²⁵, as well as by examining the THz polarization under specific polarization combinations of two-color fields²⁶.

In this work, according to the classical trajectory Monte-Carlo (CTMC) method, we elucidate how various types of electron-core interactions, including soft collisions and re-collisions, are imprinted in the TWG polarization. Meanwhile, it reveals the equivalence between the THz polarization and asymmetry pointer of photoelectron momentum distributions (PMDs), which can be substantially employed for the reconstruction of atomic core potentials.

Coulomb effect on THz wave emission

In CTMC method, within an ensemble of trajectories $\{i\}$, the i th trajectory $\mathbf{r}_i(t)$ is determined by solving the equation of motion $\mathbf{a}_i(t) \equiv \partial^2 \mathbf{r}_i(t) / \partial t^2 = -\mathbf{E}(t) - \nabla V[\mathbf{r}_i(t)]$ starting from the initial tunneling time $t_0^{(i)}$. The initial conditions and ionization rate w_i of the CTMC method are detailed in *Supplement Sec. 2*. The radiation derives from the acceleration of the ensemble $\mathbf{a}(t) = \sum_i w_i \Theta(t - t_0^{(i)}) \mathbf{a}_i(t)$ with $\Theta(t)$ the Heaviside function^{27,28}. The time-domain THz wave is obtained by evaluating $\mathcal{F}^{-1}\{\mathcal{W} \mathcal{F}\{\mathbf{a}(t)\}(\omega)\}(t)$ with \mathcal{F} the Fourier transform and \mathcal{W} the low-pass filter.

Taking the two-color bi-circularly polarized fields for instance, once the electron is released from the atom, its trajectory, compared to the path $\mathbf{r}_0(t)$ driven solely by the external light field, may become a bent one $\mathbf{r}(t)$ in the presence of Coulomb interaction, as shown in Fig. 1(a). The Coulomb effects on each trajectory eventually alters the global distribution of

the electronic wave packet. Fig. 1(b) shows the ensemble of trajectories when the Coulomb potential is absent. At an arbitrary time t , the positions of all classical trajectories, $r_0^{(i)}(t)$, correspond to the spatial distribution of photoelectron wave packet. The radiation is induced by the ensemble acceleration $\langle \mathbf{a}_0(t) \rangle = -\mathbf{E}(t)n(t)$, showing a consistent form to the PC model¹⁶, but with the electron density $n(t) = \sum_i w_i \Theta(t - t_0^{(i)})$ as a sum over all trajectories. When the parent ion is present, the distribution of trajectories is slightly distorted as shown in Fig. 1(c). The distortion may result in observable patterns in PMD, and also equips the acceleration with a correction term, $\langle \mathbf{a}(t) \rangle = \langle \mathbf{a}_0(t) \rangle + \langle \mathbf{a}_C(t) \rangle$, with $\langle \mathbf{a}_C(t) \rangle = \sum_i w_i \Theta(t - t_0^{(i)}) \frac{\mathbf{r}_i(t)}{|\mathbf{r}_i(t)|^3}$ from the Coulomb potential, inducing extra modulation in radiation.

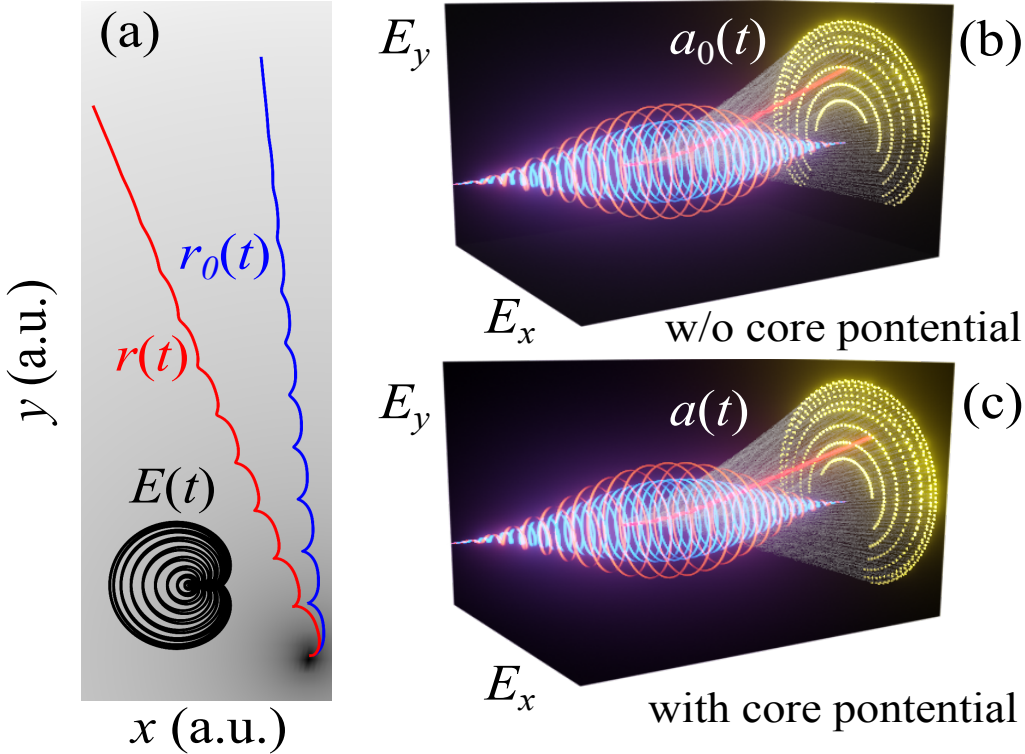


Figure 1: The influence of Coulomb interaction on photoelectron trajectories. Panel (a) shows an exemplary trajectory of photoelectron, either subjected to the Coulomb potential (red) or not (blue). Panels (b) and (c) show the distribution of photoelectron wave packet as an ensemble of classical trajectories with and without Coulomb interaction as indicated.

We explore TWG in two-color fields by mixing the fundamental of a Ti:sapphire laser [800 nm (ω), 35 fs] with its second harmonic [400 nm (2ω), circularly polarized]. The ω and 2ω beams have intensities of $I=1.5 \times 10^{14}$ W/cm² and $I/2$, respectively. As schematically demon-

strated in Fig. 2(a), we measure the THz yield $S(\varepsilon, \phi)$ as a function of ε , the ellipticity of ω beam, and ϕ , the interpulse phase delay. The TWGs are detected with electro-optic sampling, and the polarization components of time-domain waveform $E_{\text{THz},\sigma}(t)$ ($\sigma \equiv x, y$) are recorded. Defining the THz peak-to-peak (PP) amplitude, $S_{\text{pp},\sigma} = \pm |\max[E_{\text{THz},\sigma}(t)] - \min[E_{\text{THz},\sigma}(t)]|$, we measure the dependence of $S_{\text{pp},\sigma}$ on $\varepsilon \in [0, 1]$ and $\phi \in [0, 2\pi]$. As the absolute time zero of ϕ is technically challenging to determine in the experiment, we further propose a method based on CTMC to determine ϕ by measuring TWG polarization directions (see subsequent parts). The detailed experimental setup, raw data and self-referencing method are presented in *Supplement Sec. 1*.

Fig. 2(b)-(g) present the distributions of $S_{\text{pp},\sigma}(\varepsilon, \phi)$ obtained from the PC model, experiment, and CTMC method. Contrary to the distribution of $S_{\text{pp},y}(\varepsilon, \phi)$ evaluated by the PC model shown in Fig. 2(c), the experimental result in (e) exhibits a bend along ε , which can be replicated by the CTMC calculation in Panel (g). The CTMC calculations without Coulomb potential show same results as the PC model, confirming the equivalence between the two methods. Thus, the bend by comparison shown in Fig. 2 is confirmed to be attributed to the Coulomb effects.

The bend of $S_{\text{pp},y}$ induced by Coulomb potential is more pronounced than that of $S_{\text{pp},x}$, because, along the y direction, the contribution of the Coulomb potential to the photoelectron momentum is comparable to the momentum induced by the laser field.

Through CTMC, the TWG is closely tied to the photoelectron wave packet as an ensemble of trajectories. The CTMC model establishes a correlation between the TWGs and PMDs. The THz emission (\mathbf{E}_{THz}) from the trajectory ensemble is expressed as the summation of individual trajectories as

$$\begin{aligned} \mathbf{E}_{\text{THz}}(\omega \rightarrow 0) &= \sum_i w_i \left(\lim_{\omega \rightarrow 0} \int_{-\infty}^{\infty} dt \frac{\partial \mathbf{v}_i(t)}{\partial t} e^{-i\omega t} \right) \\ &= \sum_i w_i \mathbf{v}_i(\infty). \end{aligned} \quad (1)$$

Here, ω represents the frequency of strong-field induced radiation, $\mathbf{v}_i(t)$ and $\mathbf{v}_i(\infty)$ denote the instantaneous velocity and asymptotic velocity (drift velocity) of the i th trajectory. The contribution of the i th trajectory to TWG is expressed as $\mathbf{E}_{\text{THz},i} \propto w_i \mathbf{v}_i(\infty)$. The polarization direction of $\mathbf{E}_{\text{THz},i}$ is defined as $\hat{\mathbf{E}}_{\text{THz},i}$, equivalent to the direction of asymptotic velocity $\hat{\mathbf{v}}_i(\infty)$. The amplitude of $\mathbf{E}_{\text{THz},i}$ is defined as $|\mathbf{E}_{\text{THz},i}| \propto |w_i \mathbf{v}_i(\infty)|$. We define the asymmetry of PMDs as $\mathbf{P}_e = \sum_i w_i \mathbf{v}_i(\infty)$ with an asymmetrical direction of $\hat{\mathbf{P}}_e$. \mathbf{E}_{THz} is proportional to \mathbf{P}_e , which is equivalent to the residual photocurrent in the PC model.

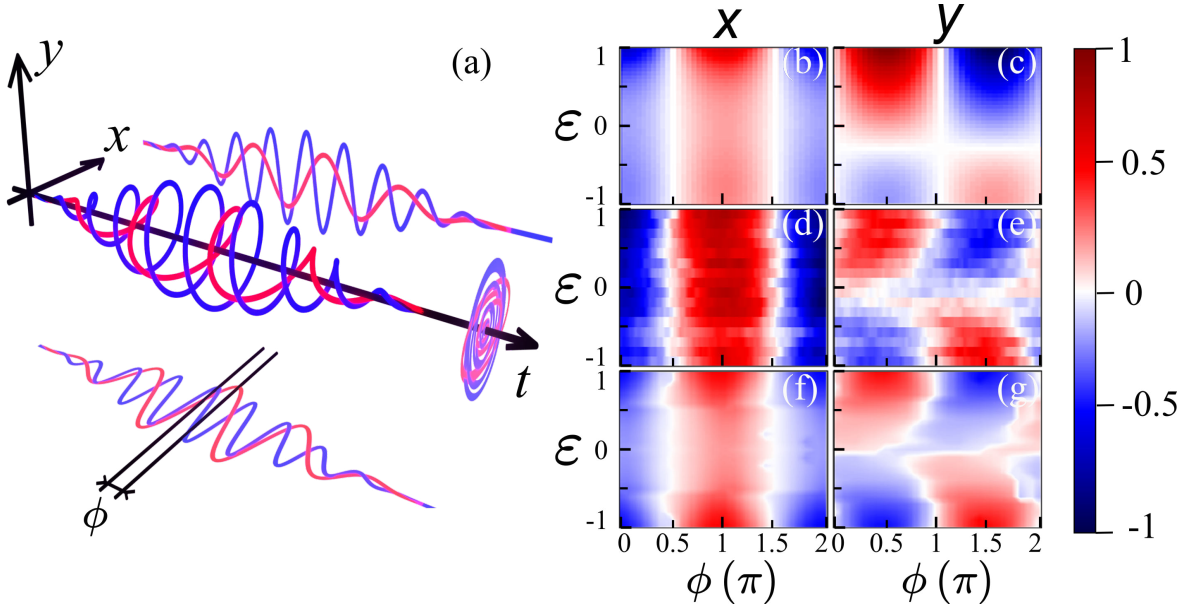


Figure 2: The THz peak-to-peak distributions in two-color fields $S_{\text{pp},\sigma}(\varepsilon, \phi)$. Panel (a) presents an illustration of the laser fields, where the ω -field (red) is elliptically polarized with a ellipticity ε and the 2ω -field (blue) is circularly polarized. The ω - 2ω phase delay is ϕ . The x direction is defined as parallel to the polarization of the ω -field when $\varepsilon = 0$ (see *Supplement Sec. 1* for detailed definition). The PP distributions in the x direction, $S_{\text{pp},x}(\varepsilon, \phi)$, are shown for (b) PC model, (d) experiment, and (f) CTMC. Correspondingly, the PP distributions in the y direction, $S_{\text{pp},y}(\varepsilon, \phi)$, are shown in Panels (c), (e), and (g).

In Figs. 3(a)-(d), we present $\hat{\mathbf{E}}_{\text{THz},i}$ and $|\mathbf{E}_{\text{THz},i}|$ of highest-weight trajectories with respect to ε and ionization instants t_0 for two selected $\phi = 0, \pi/2$. Figs. 3(e)-(h) analyze the TWGs from the trajectory ensemble, where the calculated $\hat{\mathbf{E}}_{\text{THz}}$, $\hat{\mathbf{P}}_e$ and measured THz polarization θ_{THz} are depicted in direct comparison with PMDs at $\varepsilon = 0, 1$. The corresponding simulation results of $\hat{\mathbf{E}}_{\text{THz},i}$, $|\mathbf{E}_{\text{THz},i}|$, $\hat{\mathbf{E}}_{\text{THz}}$, $\hat{\mathbf{P}}_e$ and PMDs without Coulomb

potential are shown in Figs. 3 of *Supplement* for comparison.

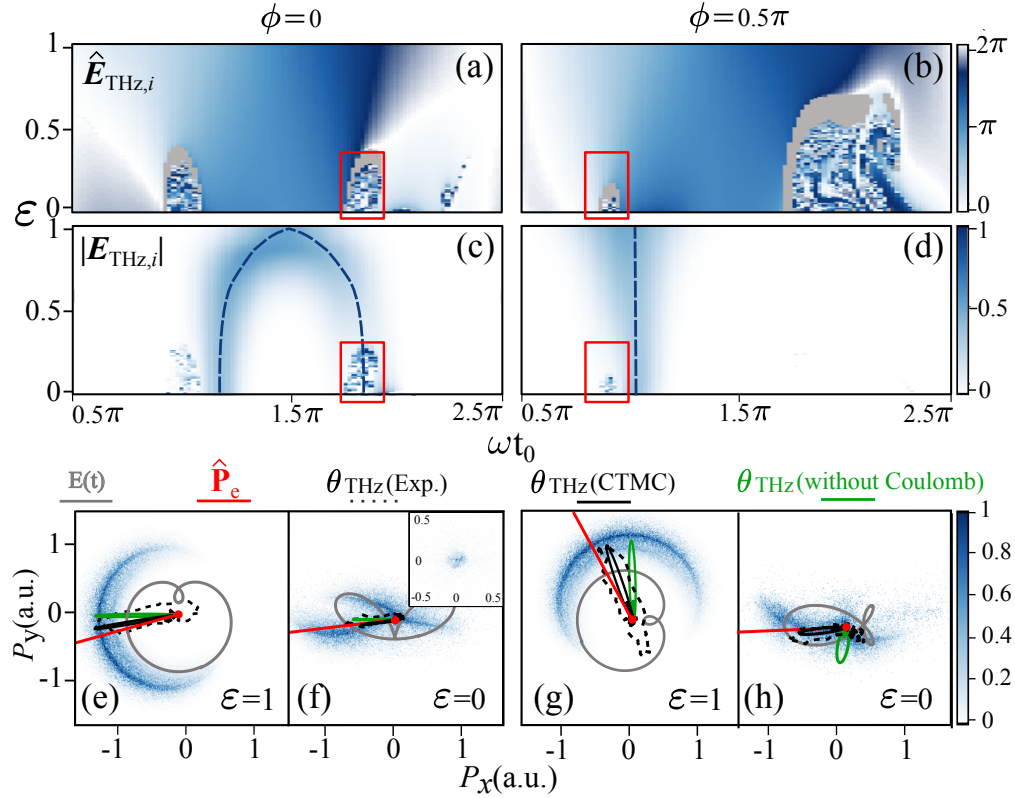


Figure 3: The trajectory analysis of THz emissions at various ellipticities ε for two selected phase delay $\phi = 0, \pi/2$. (a)-(d) Contribution of the i th individual trajectory to THz emission $\mathbf{E}_{\text{THz},i}$ with respect to ε and ionization instants t_0 . Panel (a) and (c) show the polarization direction $\hat{\mathbf{E}}_{\text{THz},i}$ and the amplitude $|\mathbf{E}_{\text{THz},i}|$ at $\phi = 0$. Panel (b) and (d) show $\hat{\mathbf{E}}_{\text{THz},i}$ and $|\mathbf{E}_{\text{THz},i}|$ at $\phi = \pi/2$. (e)-(h) THz emissions from the trajectory ensemble \mathbf{E}_{THz} . The PMDs, laser electric fields (grey bold lines), THz polarization $\hat{\mathbf{E}}_{\text{THz}}$ with (black solid lines) or without (green solid lines) Coulomb potential, asymmetry pointer of PMDs $\hat{\mathbf{P}}_e$ (red solid lines) and the experimental THz polarization θ_{THz} (dashed lines) are presented for comparison. The inset in Panel (f) depicts the PMD of selected trajectories in the red box in Panels (a) and (c).

For large ellipticities $\varepsilon > 0.4$, Figs. 3(a) and (b) illustrate that $\hat{\mathbf{E}}_{\text{THz},i}$ smoothly changes with respect to t_0 . In Figs. 3(c) and (d), the maxima of $|\mathbf{E}_{\text{THz},i}|$ correspond to the peak values of the two-color fields (dashed lines), where the tunneling ionization rate reaches its maximum. These maxima represent the main tunneling temporal windows. Figs. 3(e) and (g) for $\varepsilon=1$ exhibit that $\hat{\mathbf{E}}_{\text{THz}}$ (black solid lines) coincides with $\hat{\mathbf{P}}_e$ (red solid lines), as predicted in Eq. (1). The angular deviations observed between $\hat{\mathbf{E}}_{\text{THz}}$ with (black solid

lines) and without (green solid lines) Coulomb potential result from the deflection of electron trajectory induced by Coulomb potential, i.e., soft collision between electron and parent ion. The angular deviation corresponds to the "streaking angle" in the "attoclock" of PMDs¹¹.

As ε decreases, chaos regions and grey regions emerge, highlighted in the red boxes in Figs. 3(a) and (b). The grey regions are explained by the scenario in which the parent core recaptures the free electron into the Rydberg state. The chaotic regions arise from the hard re-collision between the electron and parent core, resulting in the emission of $\hat{\mathbf{E}}_{\text{THz},i}$ occurring near-isotropically across all 4π solid angles. Trajectories within chaos regions that do not overlap with the maximum region of $|\mathbf{E}_{\text{THz},i}|$, as depicted in Figs. 3(b) and (d), contribute minimally to TWGs due to their low weight. However, when the chaos region overlaps with the right branch of tunneling windows, as red boxed in Panel (a) and (c), the re-collision trajectories significantly influence the TWGs. The isotropic and isotropic distribution of $\hat{\mathbf{E}}_{\text{THz},i}$, as shown in the inset of Panel (f), leads to the counterbalancing of contributions from individual trajectories. In Fig. 3(f), the angular deviations between $\hat{\mathbf{E}}_{\text{THz}}$ with and without Coulomb potential cannot be observed as in the case of $\varepsilon = 1$. It can be explained by the scenario that, although $\hat{\mathbf{E}}_{\text{THz},i}$ are deflected by Coulomb potential, yet the high-weight trajectories within the right branch of tunneling windows do not contribute to the TWGs, the Coulomb potential thus is not effectively manifest in the TWGs.

When ε changes from 1 to 0, the electron-core interaction transitions from soft collision to hard re-collision, manifested in the ϕ -dependent TWGs. In hard re-collision, the random scattering breaks the homogeneous behavior of trajectory ensemble, diminishing the effectiveness of encoding dynamics and structural information in the TWGs. In contrast, during a soft collision, the Coulomb potential deflects the trajectory ensemble while maintaining its homogeneous behavior. In this scenario, the trajectory ensemble can be approximately represented by the highest-weight trajectory, providing a more straightforward basis for reconstructing electron dynamics. This analysis can be further simplified by an analytical solution obtained through perturbatively evaluating the Coulomb-induced correction to the

guiding center trajectory, where the fast timescale laser-induced oscillation is averaged out²⁹. Refer to *Supplement* Eqs. S5 and S6, and S15 for more details.

Reconstruction of unknown potential by THz radiation

The all-optical reconstruction of the core potential of generating medium is conceptually straightforward. If a sufficiently broad spectrum of the radiated field, $\tilde{\mathbf{E}}_{\text{rad}}(\omega)$, can be acquired, the reconstructed acceleration of photoelectron, $\mathbf{a}(t) = \mathbf{E}_{\text{rad}}(t)$, in principle, allows tracing the local potential, $\nabla V(\mathbf{r}) = -\mathbf{a}_C(\mathbf{r}(t)) = -[\mathbf{a}(t) + \mathbf{a}_0(t)]$. Multiple trajectories under different phase delay ϕ , therefore, sketch the contour of $\nabla V(\mathbf{r})$ as analogous to the mesh representation of an object in an artistic wire sculpture (See *Supplement* Sec.5 for details).

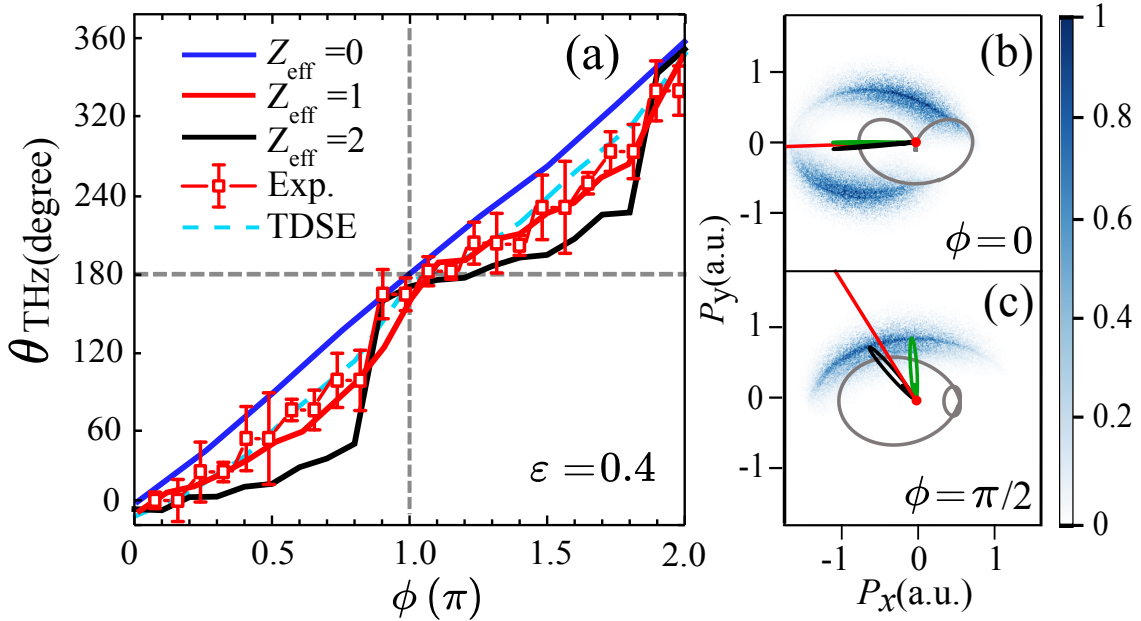


Figure 4: Reconstruction for the effective Coulomb potential with THz polarizations. (a) Dependence of the THz polarization direction $\theta_{\text{THz}}(\phi)$ on time delay ϕ with different effective charge Z_{eff} at $\epsilon=0.4$. (b) and (c) the same plots as Fig. 3 (e)-(h), but for $\epsilon=0.4$, $Z_{\text{eff}}=1$ at $\phi=0$ and $\pi/2$ respectively.

The acceleration \mathbf{a}_C induced by Coulomb potential becomes significant only when the electron-nucleus distance $\mathbf{r}(t)$ is very small. Consequently, Coulomb potential seriously mod-

ifies the TWG during the initial phase when the electron has just departed from the core after ionization. The TWG modification within a narrow temporal windows corresponds to the high-frequency component of THz emissions. Theoretical testing suggests that the accurate reconstruction of the entire profile of the Coulomb potential would necessitate a broad-spectrum THz coverage up to 280 THz. However, despite recent significant advancements in generating and detecting broadband THz emissions in gas plasma, the capabilities of TWG generation and detection remain restricted to 100 THz.

The practical limitation in our setup allows for reliable measurement only from 0.1 to 3 THz. Fortunately, the TWG is determined by the slow timescale dynamics that are highly sensitive to the initial stage of the photoelectron motion. As the interaction with the parent ion can dramatically alter the photoelectron trajectory when the electron roams around the core within a short time after the tunneling ionization, it is hence still possible to extract partial information by exploiting the TWG.

It can be shown by an example to retrieve a key parameter of the effective potential. We assume a Coulomb potential $V(\mathbf{r}) = -\frac{Z_{\text{eff}}}{|\mathbf{r}|}$ with Z_{eff} the effective charge, which reflects the strength of the Coulomb potential, to be determined.

The polarization direction of TWG as a function of phase delay ϕ , i.e. $\theta_{\text{THz}}(\phi)$, can be experimentally measured by scanning ϕ . The absolute ϕ can be determined by comparing the measurement and theories, including CTMC and direct solution of the time-dependent Schrödinger equation (TDSE). As shown in Fig. 4(a), $\theta_{\text{THz}} = 0^\circ, 180^\circ$ at $\phi = 0^\circ, 180^\circ$ remains identical regardless of Z_{eff} , establishing a criterion for determining the absolute ϕ (see *Supplement S.7* for detailed calibration).

As shown in Fig. 4(a), $\theta_{\text{THz}}(\phi)$ possesses a high correlation with Z_{eff} , allowing for the determination of Z_{eff} by comparing the experimentally obtained $\theta_{\text{THz}}(\phi)$ with the simulation one. Figs. 4(b) and (c) presents the same plots as Fig.3 (e)-(h) for $\varepsilon = 0.4$, $\phi = 0, \pi/2$ as a further inspection of the comparison of TWG polarization and angular streaking in PMDs. In Fig. 4, both θ_{THz} and $\hat{\mathbf{P}}_e$ are rotated as a function of ϕ , establishing a connection between

our measurement and the "phase-of-phase (POP) attoclock" experiment³⁰. $\theta_{\text{THz}}(\phi)$ in our measurement and the emitting angle in "POP attoclock" show the similar evolution with respect to ϕ , validating the reconstruction methodology based on TWGs. The congruence implies the THz polarization measurements could serve as an alternative to the "POP attoclock", providing a potential avenue for extracting tunneling ionization dynamics in future studies.

Conclusion

In this work, we found that the dependence of THz yields on the ellipticity and interpulse phase delay of bi-chromatic laser cannot be explained by the PC model due to the absence of the photoelectron-core interaction. The inclusion of Coulomb potential in the CTMC model not only reproduces the experimental results but also establishes the connection between THz radiation and photoelectron motion. Compared to the re-collision scenario at low ellipticity, the structure information is more efficiently encoded in the motion of trajectory ensemble after a soft collision at intermediate ellipticity. Therefore, with the support of CTMC and TDSE simulation, we introduce a reconstruction methodology for extracting local potential by measuring THz polarizations with respect to the two-color phase delay. The THz polarization is equivalent to the asymmetry pointer of PMDs, connecting our measurement and "attoclock" of PMDs. In contrast to the angular offset in the conventional "attoclock", our experiment allows for a precise and easy-to-implement determination of THz polarization. Furthermore, TWGs emitted from condensed-phase media provide an opportunity to extract electron motion and structure in the bulk solid or liquid targets.

Acknowledgement

This work was supported by the National Key Research and Development Program of China (No. 2022YFA1604302) and the National Natural Science Foundation of China (No.

12334011, No. 12174284, and No.12374262). We acknowledge the computational resource of the HPC platform in ShanghaiTech University.

References

- (1) Itatani, J.; Levesque, J.; Zeidler, D.; Niikura, H.; Pépin, H.; Kieffer, J. C.; Corkum, P. B.; Villeneuve, D. M. Tomographic imaging of molecular orbitals. *Nature* **2004**, *432*, 867–871.
- (2) Vozzi, C.; Negro, M.; Calegari, F.; Sansone, G.; Nisoli, M.; De Silvestri, S.; Stagira, S. Generalized molecular orbital tomography. *Nat. Phys.* **2011**, *7*, 822–826.
- (3) Shafir, D.; Soifer, H.; Bruner, B. D.; Dagan, M.; Mairesse, Y.; Patchkovskii, S.; Ivanov, M. Y.; Smirnova, O.; Dudovich, N. Resolving the time when an electron exits a tunnelling barrier. *Nature* **2012**, *485*, 343–346.
- (4) Pedatzur, O.; Orenstein, G.; Serbinenko, V.; Soifer, H.; Bruner, B. D.; Uzan, A. J.; Brambila, D. S.; Harvey, A. G.; Torlina, L.; Morales, F.; Smirnova, O.; Dudovich, N. Attosecond tunnelling interferometry. *Nat. Phys.* **2015**, *11*, 815–U184.
- (5) Lein, M. Attosecond Probing of Vibrational Dynamics with High-Harmonic Generation. *Phys. Rev. Lett.* **2005**, *94*, 053004.
- (6) Baker, S.; Robinson, J. S.; Haworth, C. A.; Teng, H.; Smith, R. A.; Chirilă, C. C.; Lein, M.; Tisch, J. W. G.; Marangos, J. P. Probing Proton Dynamics in Molecules on an Attosecond Time Scale. *Science* **2006**, *312*, 424.
- (7) Bian, X.-B.; Bandrauk, A. D. Probing Nuclear Motion by Frequency Modulation of Molecular High-Order Harmonic Generation. *Phys. Rev. Lett.* **2014**, *113*, 193901.
- (8) Cook, D. J.; Hochstrasser, R. M. Intense terahertz pulses by four-wave rectification in air. *Opt. Lett.* **2000**, *25*, 1210–1212.

- (9) Brunel, F. Harmonic generation due to plasma effects in a gas undergoing multiphoton ionization in the high-intensity limit. *J. Opt. Soc. Am. B* **1990**, *7*, 521–526.
- (10) Huang, Y.; Meng, C.; Wang, X.; Lü, Z.; Zhang, D.; Chen, W.; Zhao, J.; Yuan, J.; Zhao, Z. Joint Measurements of Terahertz Wave Generation and High-Harmonic Generation from Aligned Nitrogen Molecules Reveal Angle-Resolved Molecular Structures. *Phys. Rev. Lett.* **2015**, *115*, 123002.
- (11) Babushkin, I. et al. All-optical attoclock for imaging tunnelling wavepackets. *Nat. Phys.* **2022**, *18*, 417–422.
- (12) Eckle, P.; Smolarski, M.; Schlup, P.; Biegert, J.; Staudte, A.; Schoeffler, M.; Müller, H. G.; Doerner, R.; Keller, U. Attosecond angular streaking. *Nat. Phys.* **2008**, *4*, 565–570.
- (13) Eckle, P.; Pfeiffer, A. N.; Cirelli, C.; Staudte, A.; Doerner, R.; Müller, H. G.; Buetiker, M.; Keller, U. Attosecond Ionization and Tunneling Delay Time Measurements in Helium. *Science* **2008**, *322*, 1525–1529.
- (14) Camus, N.; Yakaboylu, E.; Fechner, L.; Klaiber, M.; Laux, M.; Mi, Y.; Hatsagortsyan, K. Z.; Pfeifer, T.; Keitel, C. H.; Moshhammer, R. Experimental Evidence for Quantum Tunneling Time. *Phys. Rev. Lett.* **2017**, *119*, 023201.
- (15) Sainadh, U. S.; Xu, H.; Wang, X.; Atia-Tul-Noor, A.; Wallace, W. C.; Douguet, N.; Bray, A.; Ivanov, I.; Bartschat, K.; Kheifets, A.; Sang, R. T.; Litvinyuk, I. V. Attosecond angular streaking and tunnelling time in atomic hydrogen (vol 568, pg 75, 2019). *Nature* **2019**, *569*, E5.
- (16) Kim, K. Y.; Glowia, J. H.; Taylor, A. J.; Rodriguez, G. Terahertz emission from ultrafast ionizing air in symmetry-broken laser fields. *Opt. Express* **2007**, *15*, 4577–4584.

- (17) Zhou, Z.; Zhang, D.; Zhao, Z.; Yuan, J. Terahertz emission of atoms driven by ultrashort laser pulses. *Phys. Rev. A* **2009**, *79*, 063413.
- (18) Zhang, K.; Zhang, Y.; Wang, X.; Yan, T.-M.; Jiang, Y. H. Continuum electron giving birth to terahertz emission. *Photonics Res.* **2020**, *8*, 760–767.
- (19) Azoury, D.; Kneller, O.; Rozen, S.; Bruner, B. D.; Clergerie, A.; Mairesse, Y.; Fabre, B.; Pons, B.; Dudovich, N.; Kruger, M. Electronic wavefunctions probed by all-optical attosecond interferometry. *Nat. Photonics* **2019**, *13*, 54.
- (20) Boutu, W.; Haessler, S.; Merdji, H.; Breger, P.; Waters, G.; Stankiewicz, M.; Frasin-ski, L.; Taieb, R.; Caillat, J.; Maquet, A.; Monchicourt, P.; Carre, B. Coherent control of attosecond emission from aligned molecules. *Nat. Phys.* **2008**, *4*, 545–549.
- (21) Zhou, X.; Lock, R.; Li, W.; Wagner, N.; Murnane, M. M.; Kapteyn, H. C. Molecular Recollision Interferometry in High Harmonic Generation. *Phys. Rev. Lett.* **2008**, *100*, 073902.
- (22) Kim, K. Y.; Taylor, A. J.; Glowina, J. H.; Rodriguez, G. Coherent control of terahertz supercontinuum generation in ultrafast laser-gas interactions. *Nat. Photonics* **2008**, *2*, 605–609.
- (23) Babushkin, I.; Skupin, S.; Husakou, A.; Köhler, C.; Cabrera-Granado, E.; Bergé, L.; Herrmann, J. Tailoring terahertz radiation by controlling tunnel photoionization events in gases. *New J. Phys* **2011**, *13*, 123029.
- (24) Liu, J.; Chen, W.; Zhang, B.; Zhao, J.; Wu, J.; Yuan, J.; Zhao, Z. Trajectory-based analysis of low-energy electrons and photocurrents generated in strong-field ionization. *Phys. Rev. A* **2014**, *90*, 063420.
- (25) Zhang, D.; Lü, Z.; Meng, C.; Du, X.; Zhou, Z.; Zhao, Z.; Yuan, J. Synchronizing Tera-hertz Wave Generation with Attosecond Bursts. *Phys. Rev. Lett.* **2012**, *109*, 243002.

- (26) Gao, Y.; Zhang, Y.; Zhang, K.; Gan, Z.; Yan, T.-M.; Jiang, Y. Coulomb potential determining terahertz polarization in a two-color laser field. *Opt. Lett.* **2023**, *48*, 2575–2578.
- (27) Zhang, Y.; Zhang, K.; Yan, T.-M.; Jiang, Y. Electron trajectory backanalysis for spectral profile in two-color terahertz generation. *J. Phys. B: At. Mol. Opt. Phys.* **2021**, *54*, 195401.
- (28) Fan, X.; Gao, Y.; Yan, T.-M.; Jiang, Y.; Zhang, Y. Trajectory analysis for low-order harmonic generation in two-color strong laser fields. *Opt. Express* **2023**, *31*, 86–94.
- (29) Dubois, J.; Berman, S. A.; Chandre, C.; Uzer, T. Capturing Photoelectron Motion with Guiding Centers. *Phys. Rev. Lett.* **2018**, *121*, 113202.
- (30) Han, M.; Ge, P.; Wang, J.; Zhenning, G.; Fang, Y.; Ma, X.; Yu, Y.; Deng, Y.; Wörner, H. J.; Gong, Q.; Liu, Y. Complete characterization of sub-Coulomb-barrier tunnelling with phase-of-phase attoclock. *Nat. Photonics* **2021**, *15*, 765–771.

TOC Graphic

